International Journal of Thermophysics, Vol. 17, No. 6, 1996

Thermal-Wave Resonant-Cavity Measurements of the Thermal Diffusivity of Air: A Comparison Between Cavity-Length and Modulation-Frequency Scans

J. Shen,[1] A. Mandelis,[1,2] and B. D. Aloysius[1]

Received February 5, 1996

The application of a thermal-wave resonant cavity to thermal-diffusivity measurements of gases has been investigated. The cavity was constructed using a thin aluminum foil wall as the intensity-modulated laser-beam oscillator source opposite a pyroelectric polyvilidene fluoride wall acting as a signal transducer. Theoretically, cavity-length and modulation-frequency scans both produce resonance-like extrema in lock-in in-phase and quadrature curves. These extrema can be used to measure the thermal diffusivity of the gas within the cavity. It was found experimentally that one can obtain very accurate and reproducible measurements of the thermal diffusivity of the gas by using simple cavity-length scanning without any signal normalization procedure, rather than traditional modulation-frequency scanning normalized by the frequency-dependent transfer function of the instrumentation. By scanning the cavity length, the thermal diffusivity of room air at 299 K was measured with three-significant figure precision as 0.216 ± 0.001 cm$^2 \cdot$ s^{-1}, with a standard deviation 0.5%. Only two significant figure accuracy could be obtained by scanning the frequency: 0.22 ± 0.03 cm$^2 \cdot$ s^{-1}, with a standard deviation of 14%. Cavity-length scanning consistently exhibited a much higher signal-to-noise ratio.

KEY WORDS: air; frequency scan; length scan; thermal diffusivity; thermal-wave resonant cavity.

1. INTRODUCTION

Thermal diffusivity is an important thermophysical parameter used in the design of heat transporting systems, which can also be used in identification

[1] Photothermal and Optoelectronic Diagnostics Laboratory and Center for Hydrogen and Electrochemical Studies, Department of Mechanical Engineering, University of Toronto, Toronto M5S 1A4, Canada.

[2] To whom correspondence should be addressed.

840/17/6-2

and diagnostics of materials of practical interest [1]. Photothermal techniques have been proven very useful in the measurement of thermal diffusivities [2–12]. The common principle of these thermal techniques consists of measuring the temperature fluctuation in a sample as a result of the nonradiative deexcitation process that takes place following the absorption of intensity-modulated radiation. Due to the fact that thermal wave propagation depends on the thermal diffusivity of the material, thermal diffusivity has been measured traditionally from the frequency- and time-domain behavior of the thermal wave in fixed-volume materials [13–15].

However, the recent development of a photopyroelectric (PPE) detector with a variable sample-to-source distance [16, 17] has introduced the possibility of measuring thermal diffusivity by monitoring the spatial behavior of the thermal wave. Subsequently, a thermal-wave cavity was built, [18] and resonance-like extrema of the thermal wave were demonstrated in both lock-in in-phase and quadrature channels when the cavity length was varied. These extrema were used to measure the thermal diffusivity of the gas within the cavity with a high precision. In this paper, we compare the novel cavity-length scanning method with the traditional frequency-scanning method for measuring the thermal diffusivity of room air within the cavity, in terms of precision of measurement, signal quality, signal-to-noise ratio, and ease of experimental implementation.

2. EXPERIMENTS

The thermal-wave resonator cavity was constructed as shown in Fig. 1. One cavity wall was simply made by mounting a 15-μm-thick aluminum foil on a circle ring so as to form a stretched, flat surface about 1 cm in diameter. The other wall was the surface of a pyroelectric polyvinylidene fluoride (PVDF) thin circular sensor, 52 μm thick and 0.8 cm in diameter. The aluminum side of the parallel-wall cavity was mounted on a micrometer stage, which allowed the cavity length, L, to vary with 10-μm step resolution. The aluminum foil surface exterior to the cavity was slightly sooted to eliminate light reflection and enhance optical absorption and thermal-wave generation from a modulated He–Ne laser, while remaining entirely thermally thin when the frequency was smaller than 30 Hz: at this frequency the thermal diffusion length in aluminum is 945 μm, which is much bigger than the thickness of the aluminum foil, 15 μm. The entirely thermally thin condition is important to achieve in practice, so as to avoid any phase lag between the intensity-modulated laser source and the appearance of the thermal wave on the other side of aluminum wall, thus increasing the controllability of the temperature oscillation inside the

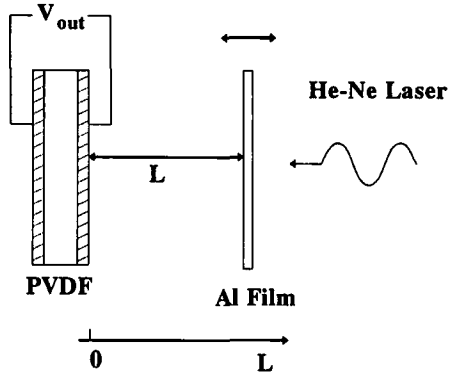

Fig. 1. Schematic diagram of the thermal wave resonant cavity.

cavity. Any additional instrumental phase lags tend to mix the lock-in amplifier in-phase (IP) and quadrature (Q) signals to some extent.

Figure 2 shows the block diagram of the experimental set up. A 10-mW He–Ne laser chopped by a mechanical chopper (EG&G Model 192) impinged normally on the aluminum surface after passing through two lenses, which expanded the laser beam to 3 mm in diameter on the aluminum foil surface to satisfy the theoretical one-dimensional assumption [16, 17]. The PVDF detector detected the thermal wave launched by the optically heated aluminum foil and produced an electrical signal. After preamplification by a low-noise preamplifier (ITHACO Model 1201), the

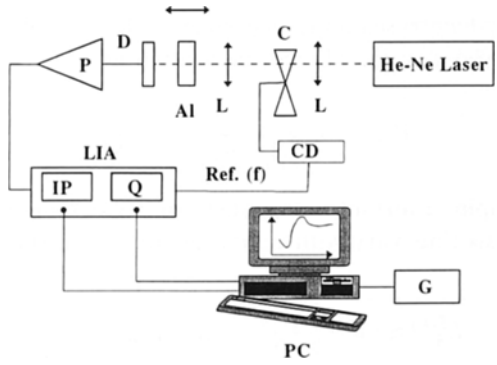

Fig. 2. Block diagram of the experimental system. L, lens; C, mechanical chopper; Al, aluminum wall of thermal-wave cavity; D, PVDF wall of thermal cavity and detector; P, preamplifier; LIA, lock-in amplifier; CD, chopper driver; PC, computer; G, plotter.

signal was fed into a lock-in amplifier (EG&G Model 5210). An IBM PC collected data from both lock-in IP and Q channels.

Since the aluminum foil is opaque, the PPE signal, under the assumption of one-dimensionality of the thermal-wave response of the cavity, can be expressed as [16, 17]

$$V(L, \alpha_g, f) = \frac{2I_0 b_{gs}}{K_p \sigma_p (1+b_{gp})(1+b_{gs})^2} \left(\frac{e^{-\sigma_s l}}{1-\gamma_{gs}^2 e^{-2\sigma_s l}} \right) \left(\frac{e^{-\sigma_g L}}{1-\gamma_{gs}\gamma_{gp} e^{-2\sigma_g L}} \right) \quad (1)$$

where

$$\sigma_j = (1+i)\sqrt{\pi f/\alpha_j} \quad (2)$$

is the complex thermal-wave diffusion coefficient; α_j denotes thermal diffusivity; $j = $ g, s, and p (g, gas; s, solid aluminum wall; p, PVDF wall); f is the modulation frequency; and l is the thickness of the aluminum foil. γ_{jk} are thermal coefficients at the (j, k) interface, defined as

$$\gamma_{jk} \equiv \frac{(1-b_{jk})}{(1+b_{jk})}, \qquad b_{jk} \equiv \frac{K_j \sqrt{\alpha_k}}{K_k \sqrt{\alpha_j}} \quad (3)$$

Here b_{jk} are the thermal coupling coefficients at the interface between media (j) and (k); K represents the thermal conductivity. The real part of Eq. (1), $\mathrm{Re}[V(L, \alpha_g, f)]$, stands for the in-phase signal, IP-PPE, while $\mathrm{Im}[V(L, \alpha_g, f)]$ stands for the quadrature signal, Q-PPE.

2.1. Cavity-Length Scanning

In the cavity-length scanning experiment, the modulation frequency f is fixed. For a given gas, Eq. (1) can be written as

$$V(L) = C \times \frac{e^{-\sigma_g L}}{1-\gamma_{gs}\gamma_{gp} e^{-2\sigma_g L}} \quad (4)$$

where C is a complex constant independent of cavity length L. The IP-PPE and Q-PPE signals thus vary with cavity length L, and their extrema occur at [18]

$$L_n^{(\mathrm{IP})} \approx \left(n - \frac{1}{2} \right) \frac{\lambda}{2}, \qquad n = 1, 2, 3, 4, \ldots \quad (5)$$

for the IP channel, and

$$L_n^{(\mathrm{Q})} \approx n \frac{\lambda}{n}, \qquad n = 1, 2, 3, 4, \ldots \quad (6)$$

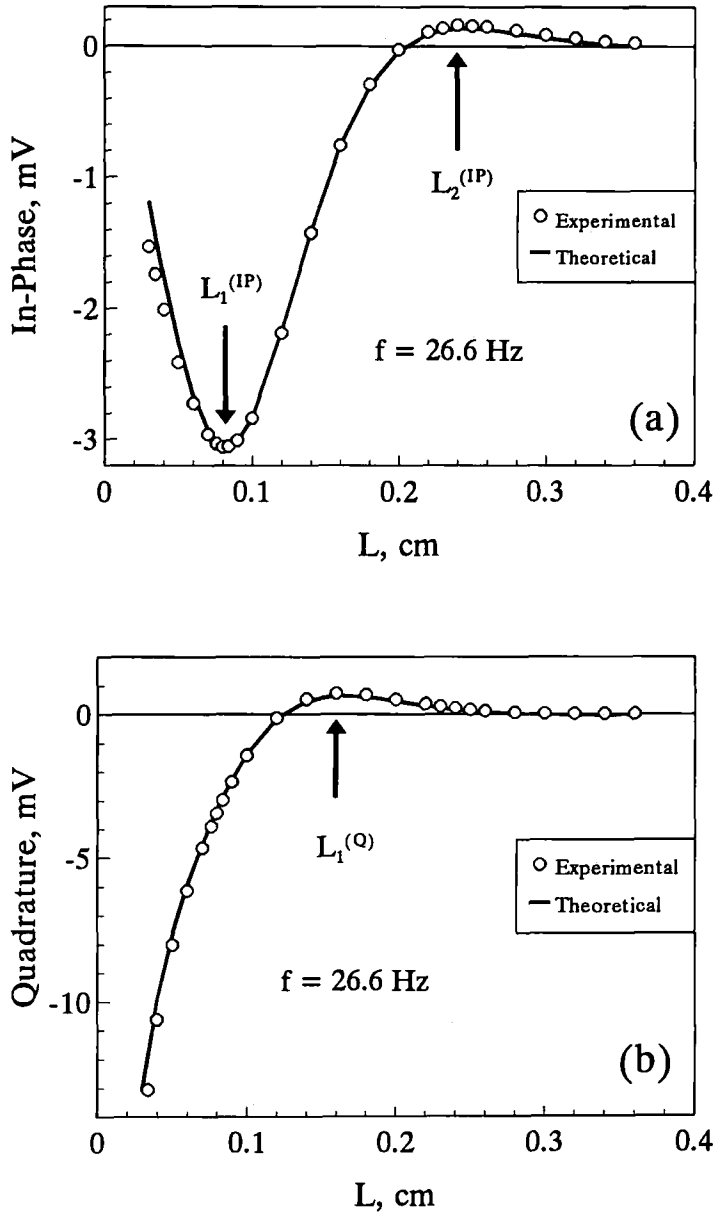

Fig. 3. Experimental and theoretical lineshapes versus thermal-wave cavity length L at a modulation frequency $f = 26.6$ Hz with a single-parameter fit, the thermal diffusivity of the ambient air $\alpha_g = 0.216\ \text{cm}^2 \cdot \text{s}^{-1}$ at $T = 299$ K. (a) IP-channel data scan; (b) Q-channel data scan.

for the Q channel, where

$$\lambda = 2\sqrt{\pi\alpha_g/f} \tag{7}$$

is the thermal-wave wavelength, corresponding to the modulation frequency f and gas thermal diffusivity α_g. The conditions for IP- and Q-channel extrema are the same as the antinodal conditions for a standing wave in a pipe resonator with a capped end and with an open end, respectively [19]. Therefore, one can imagine that the thermal-wave cavity acts like a resonator, when the phase of the thermal wave returns to its original value (plus an integral multiple of 2π) after one round-trip in the cavity.

Thermal diffusivity, therefore, can be *determined* by the location of these extrema. Owing to the exponential decay of the thermal wave in space, only the $n=1$ and, perhaps, $n=2$ resonances are important in practice, shown in Fig. 3. From Eqs. (5), (6), and (7) we have

$$\alpha_g = \frac{f}{\pi}(L_2^{(IP)} - L_1^{(IP)})^2, \qquad \alpha_g = \frac{4f}{\pi}(L_1^{(Q)} - L_1^{(IP)})^2, \qquad \alpha_g = \frac{4f}{\pi}(L_2^{(IP)} - L_1^{(Q)})^2 \tag{8}$$

Numerical calculations, presented in Table I, show that although these resonance positions (columns 3, 4 and 5) are not exactly the same as Eqs. (5) and (6), their differences are almost exactly equal to quarter (columns 7 and 8)- or half-wavelength (#6) and do not depend on the value of frequency and the type of gas present. Therefore, any of the Eqs. (8) can be used to measure the thermal diffusivity of the gas within the cavity. This relative measurement eliminates the requirement for accurate knowledge of

Table I. Theoretical Calculation of Thermal-Wave Cavity-Length Scans

Gas	f (Hz)	$L_1^{(IP)}/\lambda$	$L_2^{(IP)}/\lambda$	$L_1^{(Q)}/\lambda$	$(L_2^{(IP)} - L_1^{(IP)})/\lambda$	$(L_2^{(IP)} - L_1^{(Q)})/\lambda$	$(L_1^{(Q)} - L_1^{(IP)})/\lambda$
Air	9.000	0.2553	0.7541	0.5040	0.4988	0.2501	0.2487
Air	26.60	0.2532	0.7524	0.5025	0.4992	0.2499	0.2493
H_2	26.60	0.2580	0.7562	0.5060	0.4982	0.2502	0.2480
Air	49.60	0.2522	0.7516	0.5015	0.4994	0.2501	0.2493
N_2	49.60	0.2523	0.7515	0.5019	0.4992	0.2496	0.2469
N_2	100.0	0.2516	0.7511	0.5011	0.4995	0.2500	0.2495
Air	100.0	0.2516	0.7514	0.5012	0.4998	0.2502	0.2496
H_2	100.0	0.2542	0.7532	0.5097	0.4990	0.2435	0.2555

Table II. Thermophysical Parameters Used in Theoretical Calculations[a]

Material	K ($W \cdot cm^{-1} \cdot K^{-1}$)	α ($cm^2 \cdot s^{-1}$)
Al	2.04	0.8418
N_2	2.620×10^{-4}	0.22044
Air	2.624×10^{-4}	0.22160
H_2	1.82×10^{-3}	1.554

[a] Quoted from Ref. 20.

the absolute value of cavity length, L, which is not an easy task. Parameters used in theoretical calculations in this paper are shown in Table II.

The precise determination of the extremal positions of the standing thermal wave is critical in the cavity-scanning experiments. PPE signals were measured versus cavity length, and an eighth-order numerical polynomial fit to the experimental data was used to find an equation describing the experimental curve. With this equation, the positions of the extrema could be precisely determined by using a computer, and the thermal diffusivity of the intracavity gas could be deduced. Referring to Eq. (8), two adjacent extrema can be used to obtain the thermal diffusivity of the ambient gas. However, it was found experimentally that using two extrema in the IP channel, $L_1^{(IP)}$ and $L_2^{(IP)}$, could yield very reproducible results, while when $L_1^{(Q)}$ in the Q channel was used the reproducibility was not so good. The superior reproducibility by using the extrema in the IP channel is probably due to the fact that the positions of extrema in the same channel shift by the same amount if noise or instrumental phase shift is introduced during the experiment. The poorer reproducibility when using adjacent extrema from two channels may be due to inexact calibration of the lock-in read-outs or because the transfer functions of two different channels are not exactly identical. Hence, the positions of the two extrema from the same channel, $L_1^{(IP)}$ and $L_2^{(IP)}$, were used to determine optimally the thermal diffusivity of the ambient air within the cavity, which was found to be 0.216 ± 0.001 $cm^2 \cdot s^{-1}$ at 299 K. Figure 3 shows the excellent agreement of the experimental data with the theoretical simulation using Eq. (4).

2.2. Frequency Scanning

In the modulation-frequency scanning experiment, a cavity length L is chosen and fixed. Similarly to the cavity-length scanning case, the correlation

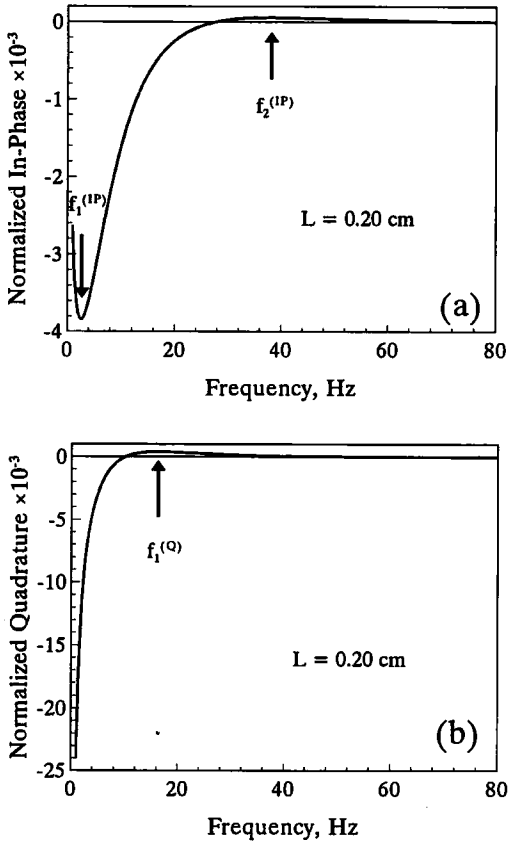

Fig. 4. Theoretical lineshape of thermal-wave cavity as a function of laser-beam modulation frequency with cavity length $L = 0.2$ cm, aluminum and PVDF walls, and gas (air) thermal diffusivity $\alpha_g = 0.22\ \text{cm}^2 \cdot \text{s}^{-1}$. (a) IP-channel signal; (b) Q-channel signal.

between the cavity length, L, and the frequency of the nth extremum in the IP channel, $f_n^{(\text{IP})}$, was found to be [18]

$$L \approx \left(n - \frac{1}{2}\right) \frac{\lambda_n^{(\text{IP})}}{2}, \qquad n = 1, 2, 3, 4, \ldots \tag{9}$$

where

$$\lambda_n^{(\text{IP})} = 2\sqrt{\frac{\pi \alpha_g}{f_n^{(\text{IP})}}} \tag{10}$$

Table III. Theoretical Calculation of Thermal-Wave Frequency Scans

Gas	L (cm)	$f_1^{(IP)}$ (Hz)	$2L/\lambda_1^{(IP)}$	$f_2^{(IP)}$ (Hz)	$2L/\lambda_2^{(IP)}$	$f_1^{(Q)}$ (Hz)	$2L/\lambda_1^{(Q)}$
Air	7.000×10^{-2}	15.79	0.3315	310.7	1.470	132.0	0.9584
H_2	7.000×10^{-2}	115.9	0.3411	2150	1.469	913.8	0.9579
Air	0.2085	2.41	0.3858	35.19	1.474	15.05	0.9640
H_2	0.2085	16.73	0.3860	243.9	1.474	104.3	0.9638
N_2	0.3085	1.22	0.4095	15.86	1.477	6.820	0.9682
Air	0.3085	1.24	0.4094	16.62	1.476	6.931	0.9679
H_2	0.3085	8.60	0.4095	111.8	1.476	48.02	0.9677

For the Q channel, the extremum condition can also be expressed as [18]

$$L \approx n\frac{\lambda_n^{(Q)}}{2}, \qquad \lambda_n^{(Q)} = 2\sqrt{\frac{\pi\alpha_g}{f_n^{(Q)}}}, \qquad n = 1, 2, 3, 4,... \tag{11}$$

In the frequency domain, the thermal-wave cavity also exhibits resonant behavior, and its extrema can be used to *measure* the thermal diffusivity of the gas in the cavity.

Similar to the cavity-length scanning, only extrema with $n = 1$ or 2 can be observed in practice, as shown theoretically in Fig. 4, in which Eq. (1) was normalized by $I_0/(K_p\sigma_p)$, the theoretical value for the PPE (reference) signal produced by direct incidence of the laser beam on and complete absorption of the PVDF detector, assumed entirely thermally thick (semi-infinite) in the frequency under consideration. The results given in Table III show that Eqs. (9) and (11) can be good approximations for the prediction of these resonance positions (columns 6 and 8), which do not change with cavity length and different gases, except for the first trough in the IP channel (column 4). The relationship between $\lambda_1^{(IP)}$ and $f_1^{(IP)}$ of this trough (columns 4) does not vary with the type of gas, but only with the cavity length L, and gradually tends to the frequency obeying Eq. (9) when L becomes large. However, this extremum is the sharpest one and has the lowest resonant frequency. It is, therefore, most suitable for measuring the thermal diffusivity of gases in the frequency-scanning experiment. When $L = 7\times10^{-2}$ cm, α_g is given by

$$\alpha_g = \left(\frac{L}{0.3315}\right)^2 \frac{f_1^{(IP)}}{\pi} \tag{12}$$

where α_g is in $cm^2\cdot s^{-1}$, L is in cm, and f is in Hz. Theoretically $f_1^{(IP)} = 15.79$ Hz, $f_2^{(IP)} = 310.7$ Hz, and $f_1^{(Q)} = 132.0$ Hz for air when

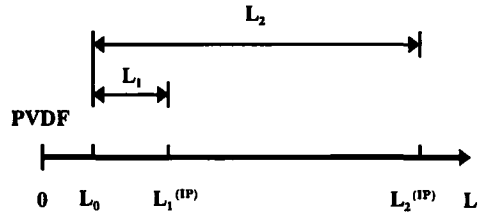

Fig. 5. Schematic diagram of the determination of the initial air gap L_0 by cavity-length scanning experiment.

$L = 7 \times 10^{-2}$ cm. It was experimentally found that the signal-to-noise ratio is good with frequencies in the range of 10 to 20 Hz. The first trough in the IP channel was therefore chosen to measure the thermal diffusivity of room air in the cavity. As the frequencies of the extrema vary with the cavity length L, L must be carefully measured in the frequency-scanning experiment.

The cavity length L may be determined by the cavity-length scanning experiment. Referring to Fig. 5, L_1 and L_2 are micrometer readings on the micrometer stage, on which the aluminum wall is mounted, measured away from an initial air gap L_0 between aluminum and PVDF walls. $L_1^{(IP)}$ and $L_2^{(IP)}$ can be written as

$$L_1^{(IP)} = L_0 + L_1, \qquad L_2^{(IP)} = L_0 + L_2 \tag{13}$$

Substituting Eqs. (13) and (7) into Eq. (5), the initial air gap L_0 can be solved for and expressed as

$$L_0 = \frac{L_2 - 3L_1}{2} \tag{14}$$

With this L_0 the cavity length $L = 7 \times 10^{-2}$ cm was set by adjusting the micrometer stage.

To take into account the transfer function of the instrumentation, which changes with the frequency, a frequency-scanning experiment was conducted, in which the intensity-modulated He–Ne laser was incident directly on the PVDF wall in the absence of the cavity. A frequency-dependent curve was thus obtained and was used to normalize the frequency-scanned experimental data with the cavity in place. Both frequency-scanned curves were fitted to 8th-order-polynomials to find numerical equations describing experimental data, and the normalization was carried out with these equations. From the normalized cavity frequency-scanning curve the frequency $f_1^{(IP)}$ corresponding to the trough

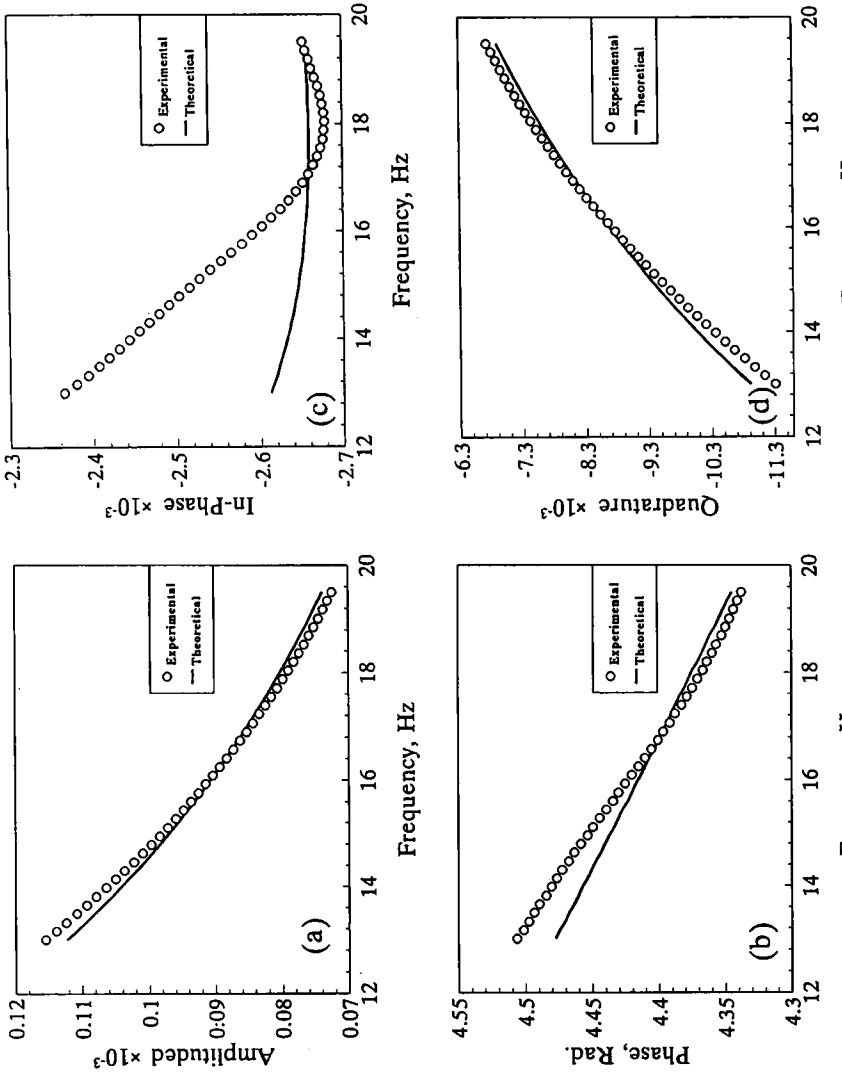

Fig. 6. Comparison of theoretical and one experimental lineshape versus modulation frequency f at cavity length $L = 7.00 \times 10^{-2}$ cm with the thermal diffusivity of the ambient air $\alpha_g = 0.25\ \text{cm}^2 \cdot \text{s}^{-1}$ measured in *this* experiment. (a) Amplitude; (b) phase; (c) in-phase; (d) quadrature.

in the IP channel was found, and the thermal diffusivity of the gas was deduced using Eq. (12). Figure 6 shows the comparison between one of the normalized experimental curves and theoretical calculation using Eq. (1), normalized by $I_0/K_p\sigma_p$, with the σ_g measured from the experiment. The agreement between the two amplitudes is close, whereas the difference of the phases is greater, especially at low frequencies. In terms of individual signal components, a sizable difference in IP channel between experimental and theoretical curves can be observed in Fig. 6c, while quadrature curves are close. Fairly large shifts, between 12.78 and 17.7 Hz, in the IP-channel extremum value of $f_1^{(IP)}$ were recorded among several repetitions of the experiments, indicating that noise was significant during the experiments. With these extremum values of $f_1^{(IP)}$ and using Eq. (12), the thermal diffusivity of room air was calculated and found to be $0.22 \pm 0.03\ \text{cm}^2 \cdot \text{s}^{-1}$.

3. DISCUSSION

In comparison with the frequency-scanning experiments, cavity-length scanning produced much more precise results and better agreement with the theory and is simple and easy to conduct. The standard deviation of α_g is about 14% of the value of α_g itself in the frequency-scanning experiments, while it is less than 1% of the value of α_g in the cavity-length scanning measurements. The reasons are as follows: First, frequency-scanning depends on the accurate knowledge of the absolute value of the cavity length L. Any error in measurement of the initial air gap L_0 by cavity-scanning will cause a disagreement between theory and experiment and a deviation in α_g. Second, as the transfer function of the instrumentation varies with frequency, accurate normalization has to be carried out, preferably during immediately successive experiments, to take the transfer function into account. Finally, any noise introduced during the measurement of the frequency-dependent transfer function of the instrumentation will be added statistically to the normalized final result of the frequency-scanning experiment, affecting the reproducibility and precision of the value of α_g. In contrast, the cavity-length scanning experiment is a relative, single measurement and not a ratio of measurements, which does not need any knowledge of initial air gap L_0 or any normalization procedure; it employs a single modulation frequency and exhibits a much higher signal-to-noise ratio and reproducibility, because the instrumental transfer function remains constant during the experiment, thus fixing the noise bandwidth throughout the scan [15]. The literature values of the thermal diffusivity of air at room temperature lie in the range of 0.19 to $0.228\ \text{cm}^2 \cdot \text{s}^{-1}$ [1, 20, 21]. The results of this work, $\alpha_g = 0.216 \pm 0.001$ and

0.22 ± 0.03 $cm^2 \cdot s^{-1}$, are in very good agreement with them and further indicate the superior sensitivity, accuracy, and resolution potential of the cavity-length scanning approach.

4. CONCLUSIONS

The thermal-wave resonant cavity offers a new degree of spatial freedom, which allows one to measure the thermal diffusivity of gases in the intracavity region by scanning the cavity length. Compared with traditional frequency scanning, this cavity-length scan method enjoys the advantages of resonant measurement at a single modulation frequency. Furthermore, no normalization is needed, which leads to a fast, precise measurement of the thermal diffusivity of gases, with less than 1% variance, compared to about 14% offered by the frequency-scan method.

ACKNOWLEDGMENTS

The authors are grateful to Natural Resources Canada and Imperial Oil Ltd. for a contract to the Center for Hydrogen and Electrochemical Studies (CHES) and a grant, respectively, which made this research possible.

REFERENCES

1. Y. S. Touloukian, R. W. Powell, C. Y. Ho, and M. C. Nicolaou, *Thermal Diffusivity* (IFI/Plenum, New York, 1973).
2. A. Mandelis and J. D. Lymer, *Appl. Spectrosc.* **39**:473 (1985).
3. P. E. Nordal and S. O. Kanstad, *Phys. Scr.* **20**:659 (1979).
4. R. Santos and L. C. M. Miranda, *J. Appl. Phys.* **52**:4192 (1981).
5. R. D. Tom, E. P. O'Hara, and D. Benin, *J. Appl. Phys.* **53**:5392 (1982).
6. W. P. Leung and A. C. Tam, *J. Appl. Phys.* **56**:153 (1984).
7. A. C. Boccara, D. Fournier, and J. Badoz, *Appl. Phys. Lett.* **36**:130 (1980).
8. W. B. Jackson, N. M. Amer, A. C. Boccara, and D. Fournier, *Appl. Opt.* **20**:1333 (1981).
9. L. C. Aamodt and J. C. Murphy, *J. Appl. Phys.* **54**:581 (1983).
10. P. K. Kuo, M. J. Lin, C. B. Reyes, L. D. Favro, R. L. Thomas, D. S. Kim, S. Y. Zhang, L. J. Inglehart, D. Fournier, A. C. Boccara, and N. Yacoubi, *Can. J. Phys.* **64**:1165 (1986).
11. P. K. Kuo, E. D. Sendler, L. D. Favro, and R. L. Thomas, *Can. J. Phys.* **64**:1168 (1986).
12. T. R. Anthony, W. F. Banholzer, J. F. Fleischer, L. H. Wei, P. K. Kuo, R. L. Thomas, and R. W. Pryor, *Phys. Rev. B* **42**: 1104 (1990).
13. A. Mandelis (ed.), *Progress in Photothermal and Photoacoustic Science and Technology, Vol. II* (Prentice-Hall, Englewood Cliffs, N.J, 1993).
14. P. K. John, L. C. M. Miranda, and A. C. Rastogi, *Phys. Rev. B* **34**:4342 (1986).
15. M. Munidasa and A. Mandelis, *Rev. Sci. Instrum.* **65**:2344 (1994).
16. A. Mandelis, J. Vanniasinkam, S. Budhuddu, A. Othonos, and M. Kokta, *Phys. Rev. B1* **48**:6808 (1993).

17. J. Vanniasinkam, A. Mandelis, S. Budhuddu, and M. Kokta, *J. Appl. Phys.* **75**:8090 (1994).
18. J. Shen and A. Mandelis, *Rev. Sci. Instrum.* **66**:4999 (1995).
19. L. E. Kinsler and A. R. Fray, *Fundamentals of Acoustics*, 2nd ed. (Wiley, New York, 1962), Chap. 8.7.
20. J. P. Holman, *Heat Transfer*, 7th ed. (McGraw–Hill, New York, 1990).
21. A. Rosencwaig, *Photoacoustics and Photoacoustic Spectroscopy* (Wiley, New York, 1980), p. 96.